ORIGINAL PAPER

Rapid adsorption of sulfamethazine on mesoporous graphene produced from plastic waste: optimization, mechanism, isotherms, kinetics, and thermodynamics

K. Mensah[1] · M. Samy[1,2] · H. Mahmoud[1,3] · M. Fujii[4] · H. Shokry[1,5]

Abstract

Sulfonamide antibiotics like sulfamethazine (SMZ) can threaten aquatic and terrestrial life even in small concentrations (≤ 1 mg/L); hence, their removal from wastewater is indispensable. However, the need to explore new promising adsorbents that are cheap, effective, and reusable also remains crucial to developing adsorption technology. This work presents a one-pot solvent-free conversion of the current most ubiquitous anthropogenic bio-resistant solid waste (plastics) into valuable carbon materials to remove SMZ from aqueous solution. High-density polyethylene waste was pyrolyzed at 500–1000 °C in an enclosed stainless-steel reactor to produce mesoporous graphene. The graphene products were characterized via microscopic and spectroscopic analyses. The effect of temperature on the graphene yield and properties was investigated. The optimum sulfamethazine (SMZ) adsorption was achieved with 600 °C carbon product (CP-600) due to its high porosity and aromatic structure. The adsorption parameters (pH, catalyst dose, and SMZ concentration) were optimized by response surface methodology (RSM) with a central composite design. 99.99% SMZ removal was achieved at 0.9 g/L adsorbent dose, 12.4 mg/L SMZ concentration, and pH 3 at 25 °C. FTIR analysis revealed that the SMZ adsorption occurred mainly via π–π/π^+–π electron interactions between the aromatic and pyrimidine rings of SMZ and the benzene ring of graphitic CP-600. The SMZ adsorption followed the pseudo-second-order kinetics, Langmuir, and Freundlich isotherm models. The adsorption was controlled by film and intraparticle diffusion and was spontaneous and endothermic. The carbon synthesized in this work is reusable and can rapidly remove more SMZ than other SMZ adsorbents.

Keywords Adsorbents · Antibiotics · Pharmaceuticals · Recycling · Wastewater treatment

✉ K. Mensah
kenneth.mensah@ejust.edu.eg

[1] Environmental Engineering Department, Egypt-Japan University of Science and Technology, New Borg El-Arab City, Alexandria, Egypt

[2] Department of Public Works Engineering, Faculty of Engineering, Mansoura University, Mansoura 35516, Egypt

[3] Department of Architecture Engineering, Faculty of Engineering, Aswan University, Aswan 81542, Egypt

[4] Department of Civil and Environmental Engineering, Tokyo Institute of Technology, Meguro-Ku, Tokyo 152-8552, Japan

[5] Electronic Materials Research Department, Advanced Technology and New Materials Research Institute, City of Scientific Research and Technological Applications (SRTA-City), Alexandria, Egypt

Introduction

Growing anthropogenic activities has led to the increasing discharge of industrial wastewater containing bio-recalcitrant toxins that can be detrimental to the environment (Samy et al. 2021; Mensah et al. 2022b). Antibiotics like sulfamethazine (SMZ) are examples of chemicals with growing market demand (Mulla et al. 2021). SMZ is an essential drug for treating various microbial infections at a low cost (Zhuang et al. 2020). However, its presence in the environment, even at small concentrations (≤ 1 mg/L), can threaten aquatic and terrestrial organisms via the generation of bacteria with antibiotic resistance genes (Poirier et al. 1999; Liu et al. 2017). Furthermore, SMZ is resistant to natural biological degradation and can bioaccumulate in the food chain causing long-term risks (Tzeng et al. 2016).

Conventional biological wastewater treatment is impotent toward SMZ degradation due to the complex nature of SMZ

(Samy et al. 2020c). Thus, several other treatment methods have been investigated to treat SMZ-containing wastewater. However, all these methods have significant drawbacks. Membrane filtration suffers from some problems such as the high energy requirement, fouling, and the generation of secondary contaminants (Samy et al. 2020c; Martínez-Sánchez et al. 2022). Moreover, advanced oxidation processes like Fenton and Fenton-like processes, electrocatalysis, photocatalysis and catalytic ozonation are expensive and the degradation of bio-resistant pollutants via these processes can result in the possible generation of toxic intermediates (Adel et al. 2020; Samy et al. 2020a).

Meanwhile, the adsorption technique provides a simple and low-cost alternative to treat pollutants (Mahanna and Samy 2020; Mensah et al. 2022a). However, the main shortcoming of this technique is the high cost of adsorbents and the reusability of the absorbent (Mensah et al. 2022a). Although adsorbents such as carbon nanotubes, zeolite, activated carbon, and chitosan have been employed to remove SMZ from aqueous solutions, it is imperative to investigate new promising precursors/adsorbents that are cheap, reusable, and effective (Mulla et al. 2021). Adsorbents like nanomaterials, MOFs, and biosorbent may require less energy to prepare but lack reusability and can remain in water after the adsorption process (Rashid et al. 2021). However, carbon char is resilient and effective and can, to some extent, be recovered from water after the adsorption process (Shokry et al. 2019). Carbon char also has a high specific surface area and remarkable internal pore structure, high adsorption capacity, low cost, good thermal, chemical and mechanical stability, high surface reactivity, high availability, environmentally friendly, flexible application, and easy to regenerate (Inyang et al. 2016; Shindhal et al. 2021). Carbon char is, therefore, the most studied adsorbent in the world (Dutta et al. 2021).

On the other hand, the production of synthetic polymers like single-use plastics has increased in recent times (Lebreton and Andrady 2019). This surge is because plastics are cheap, resistant to chemicals, light weighed, and thermally and electrically non-conductive (Van Franeker and Law 2015; Geyer et al. 2017). Plastic production has grown from 23 million tonnes in 1967 to around 348 million tonnes, with an annual growth rate of nearly 10% (Plastic Europe 2018; Bolívar-Subirats et al. 2021). The packaging sector is the dominant user of plastic polymer and generates an enormous quantity of plastic waste (141 million tonnes out of the total 319 million tonnes produced plastics) (Plastic Europe 2018; Rhodes 2018). Therefore, about half of all waste plastic resins are produced for packaging purposes and used once in a short

period (Plastic Europe 2018; Rhodes 2018). Consequently, around 20–30% of municipal solid waste is composed of plastics (5–15% by mass) (Lebreton and Andrady 2019). Currently, 12% of global plastic waste is incinerated, 79% is discarded, and only 9% is recycled (Geyer et al. 2017; Powell and W 2019).

The complex nature of plastic polymers like high-density polyethylene (HDPE) and their resistance to several chemicals make plastics recalcitrant to various natural degradation cycles, thus posing major environmental challenges (Geyer et al. 2017; Thushari and Senevirathna 2020). Lightweight plastic can float on the surface of waters and reduce sunlight penetration needed for photosynthesis by aquatic plants (Kühn et al. 2015). This retards aquatic plants' growth and can even threaten aquatic life. Organisms that depend on these plants for food are negatively affected (Van Franeker and Law 2015). Furthermore, suspended plastics serve as breeding habitats for insects and mosquitoes that transmit diseases such as malaria. Moreover, they are a source of obstruction in pipes and drains, resulting in waterlogging (Rochman et al. 2016). Another pressing issue of plastic waste is the production of secondary microplastics. Plastic debris, both terrestrial and marine, fragments into tiny particles over a period when exposed to the weather, eventually becoming microplastics (Isobe et al. 2017; Hahladakis et al. 2018). However, microplastics are tiny and are easily ingested by many creatures in the aquatic environment. This poses a significant risk to the organisms since the consumption of these tiny plastic particles has been linked to pathological stress, false satiation, reproductive difficulties, restricted enzyme synthesis, decreased growth rate, and oxidative stress (Hahladakis et al. 2018). Microplastics can also absorb hazardous compounds from the surrounding water and then enter the food chain (Isobe et al. 2017).

Meanwhile, recycling such waste plastics provides a sustainable approach for managing the quantity of waste plastics and generating socio-economic benefits (Rhodes 2018). Previous literature has demonstrated the conversion of waste plastics into value-added products such as fuels, carbon nanotubes, carbon spheres and porous carbons for energy and energy storage, adsorption, catalyst, lubrication reducing agents in extractive metallurgy (Pol and Thiyagarajan 2010; El Essawy et al. 2017; Zhang et al. 2018; Asante et al. 2020; Tournier et al. 2020). However, HDPE is scarcely recycled, and the literature did not pay great attention to the valuable solid carbon-rich materials obtainable from HDPE pyrolysis and its characteristics and possible applications. HDPE contains

a substantial amount of carbon (about 85%) and volatile matter (around 99%) (Dankwah and Koshy 2014). This property makes HDPE waste an excellent candidate for recycling technologies (Asante et al. 2020; Nimako et al. 2020). Furthermore, HDPE waste is abundantly available to serve as a cheap source of carbon precursor (Eriksen et al. 2014; Rhodes 2018; Lebreton and Andrady 2019). HDPE waste may include detergent bottles, milk jugs, and molded plastic cases (Rhodes 2018).

Consequently, this work focused on one-pot solvent-free pyrolysis of the current most ubiquitous anthropogenic bio-resistant solid waste (plastics) into promising carbon materials for SMZ adsorption from aqueous solutions. The first part of the study discussed the effect of temperature on HDPE pyrolysis, while the latter discussed the removal of SMZ from an aqueous solution with the prepared carbon materials. This study involved the application of response surface methodology (RSM) to optimize the operating conditions and establish the interactions between the SMZ removal efficiency and operating parameters. This work further studied the adsorption mechanism, kinetics, isotherms, and thermodynamics to deeply understand the adsorption behavior. The adsorbent recyclability was also examined, and the performance of the prepared adsorbent in this work was compared with other recently produced SMZ adsorbents.

Materials and methods

Materials

Empty HDPE [$(C_2H_4)_n$] plastic bottles from cosmetic products and drinking bottles were gathered from domestic and municipal waste. SMZ (99%, $C_{12}H_{14}N_4O_2S$) was purchased from Alfa Aesar (USA), hydrochloric acid (37%, HCl) was procured from Merck KGaA (Germany), sodium hydroxide pellets (98%, NaOH) were purchased from Piochem (Egypt), methanol (99%, CH_3OH) was acquired from TEDIA (USA), and sodium chloride salt (NaCl) was obtained from Alpha Chemika (India).

Batch pyrolysis of HDPE

The HDPE waste (HDPE-W) was washed thoroughly with water and sun-dried. The HDPE-W was then cut into pieces, and 10 g of the shredded HDPE-W was loaded into a 420-mL stainless-steel autoclave and placed in a muffle furnace

(ASH AMF 25 N electric muffle). The autoclave jar was tightly sealed to retain all gaseous compounds produced from the thermochemical reaction and prevent air pollution. The pyrolysis reaction was initiated at a heating rate of 27 °C/min in the presence of nitrogen gas until reaching the targeted temperature. The pyrolysis was continued at the target temperature for 2 h and left to cool overnight. The char product (CP) was then weighed immediately to estimate its yield using Eq. 1. The CP was finally stored in a desiccator for further applications. The CP was labeled as CP followed by the thermolysis temperature. For instance, CP-500 refers to char produced at 500 °C.

$$Yield = \frac{Weight \ of \ CP}{Dry \ weight \ of \ HDPE \ precursor} \times 100\% \tag{1}$$

Batch SMZ adsorption studies

A 200 mg/L stock solution of SMZ was prepared by dissolving 0.2 g of SMZ solid in 1000 mL of deionized water. An initial study was conducted to assess the adsorption activity of the prepared carbon materials and select the carbon material with the highest performance using 10 mg/L SMZ solution, 1 g/L adsorbent dose, and pH 7 at room temperature. The removal efficiency was calculated using Eq. 2.

$$R\% = \frac{(C_0 - C_t)}{C_0} \times 100\% \tag{2}$$

Details of the experimental design of the response surface methodology (RSM) are presented in Text S1, while that of the adsorption isotherms, kinetics, and thermodynamics are discussed in Text S2, Text S3, and Text S4, respectively. The analytical methods are described in Text S5.

Characterization and analytical methods

A scanning electron microscope (SEM) (JEOL, JSM-6010LV, Japan) was used to examine the surface morphology of the prepared materials. Detailed morphology and elemental composition were acquired using a transmission electron microscope (TEM) equipped with an energy-dispersive X-ray spectrometer (EDX) (JEOL, JEM-2100F, Japan). Carbon (C), hydrogen (H), nitrogen (N), and sulfur (S) content were analyzed using Elementar (Germany) Vario Micro cube. X-ray diffraction (XRD) (Bruker D2 Phaser) was used to obtain crystallographic information

about the prepared adsorbents. The specific surface area and porosity of the prepared adsorbents were examined using Brunauer–Emmett–Teller (BET) method with N_2 gas adsorption at 77 K, and the pore size distribution was analyzed by Barrett, Joyner, and Halenda (BJH) method (Microtrac MRB Belsorp Mini X, Japan). The samples were degassed at 180 °C overnight before the analysis using Belprep Vac 3. Fourier transform infrared analysis (FTIR 8400 s, Shimadzu, Japan) was used to determine the adsorbent surface functional groups before and after adsorption. The pH_{pzc} of the most effective adsorbent prepared in this work was determined using the pH drift method as reported in our previous work (Mensah et al. 2022a). The SMZ concentration was quantified using an HPLC system (Agilent 1200 series, USA) with XDB C-18 (4.6×150) column as discussed in our previous work (Samy et al. 2020c). The detection limit was 0.0361 mg/L.

Results and discussion

Yield of CP

Pyrolysis was adopted in this work because it is flexible (easily manipulatable to optimize product yield) and environmentally friendly (Pol et al. 2009b). The pyrolysis mechanism involves the dissociation of long polymeric chains of the plastic dissociates into low molecular weight liquid, gases, and char. C–H and C–C bonds break down to release solid carbon and hydrogen or hydrocarbon gases (Pol et al. 2009a; Zhuo and Levendis 2014). The carbon sheets settle on a surface at an autogenic pressure, while the present gases act as reducing agents to keep the carbon in solid form and segregated during cooling (Pol 2010; Zhuo and Levendis 2014; Mensah et al. 2021).

The product yield is crucial to the economics of every fabrication process; thus, the production of CP was optimized by the pyrolysis temperature. The yield results (Fig. S1) reveal that only about 5% of CP-500 was produced, indicating a lack of carbon growth due to insufficient C–H and C–C breakdown at 500 °C (Pol et al. 2009b; Mensah et al. 2021). This outcome further suggests that several gaseous hydrocarbons remained after the pyrolysis. A significant improvement of the CP yield (~ 16%) was observed at CP-600. Studies have shown that almost all C-H and C–C bonds of hydrocarbons break down at 600 °C under autogenic pressure and carbon remains solid after the pyrolysis (Mensah et al. 2021). Therefore at 600 °C, the significant dissociation of gaseous

hydrocarbons caused an increment in the yield of CP-600. A slight improvement in the yield was achieved when the pyrolysis temperature was increased to 700 °C (~ 17%), while no significant change was observed beyond this temperature. Therefore, 600 °C is economically selected as the optimum temperature for carbon production from HDPE since increasing temperature above 600 °C did not report any considerable increase in yield. This observation is consistent with a previous study where no increase in autogenic pressure was observed after 600–700 °C during the thermal decomposition of mesitylene due to a lack of further dissociation of gaseous hydrocarbons (Pol and Thiyagarajan 2009).

Characteristics of CP

The thermal decompositions of HDPE produced CPs with varying morphologies. The SEM micrographs of CP-500 and CP-600 show agglomerated amorphous structures with non-uniform shapes and sizes (Fig. S2a and S2b). The TEM micrographs of CP-500 and CP-600 reveal layers of graphene sheets entangled and rippled together (Fig. 1a and 1b). The shadows and dark portions depict the agglomeration of graphene sheets of the CP-500 and CP-600. However, CP-600 has few rippled morphologies indicating an improvement in graphitization with temperature. The formation of graphene is associated with the assembly of hexagonal rings of carbon released from the pyrolysis of HDPE (Pol et al. 2009a; Zhuo and Levendis 2014). CP-700 exhibited a blend of spherical and amorphous morphologies (Fig. S2c). The TEM micrograph of CP-700 shows dark spheres of solid carbon (Fig. 1c). At autogenic pressure, carbon spheres are produced when carbon sheets settle on the surface of preformed circular carbon nuclei (Pol 2010; Mensah et al. 2021). The highly pressurized system at 700 °C pyrolysis and reducing agents such as CO_2 and C-H gases ensured the solid spherical morphology was maintained (Pol 2010; Mensah et al. 2021). CP-800 exhibited similar blends of carbon spheres and amorphous graphene (Fig. S2d and 1d). CP-900 and CP-1000 contain fiber-like structures that emerge with amorphous graphene (Figs. S2e and S2f). TEM micrographs revealed the presence of hollow tubular structures of CNT in CP-900 and CP-1000 (Fig. 1e and f). The growth of CNT was more in CP-1000, indicating that temperature played a crucial role in the CNT formation. Noticeably, various carbon morphologies ranging from amorphous carbon, agglomerated graphene sheets, carbon microspheres (CMS), and
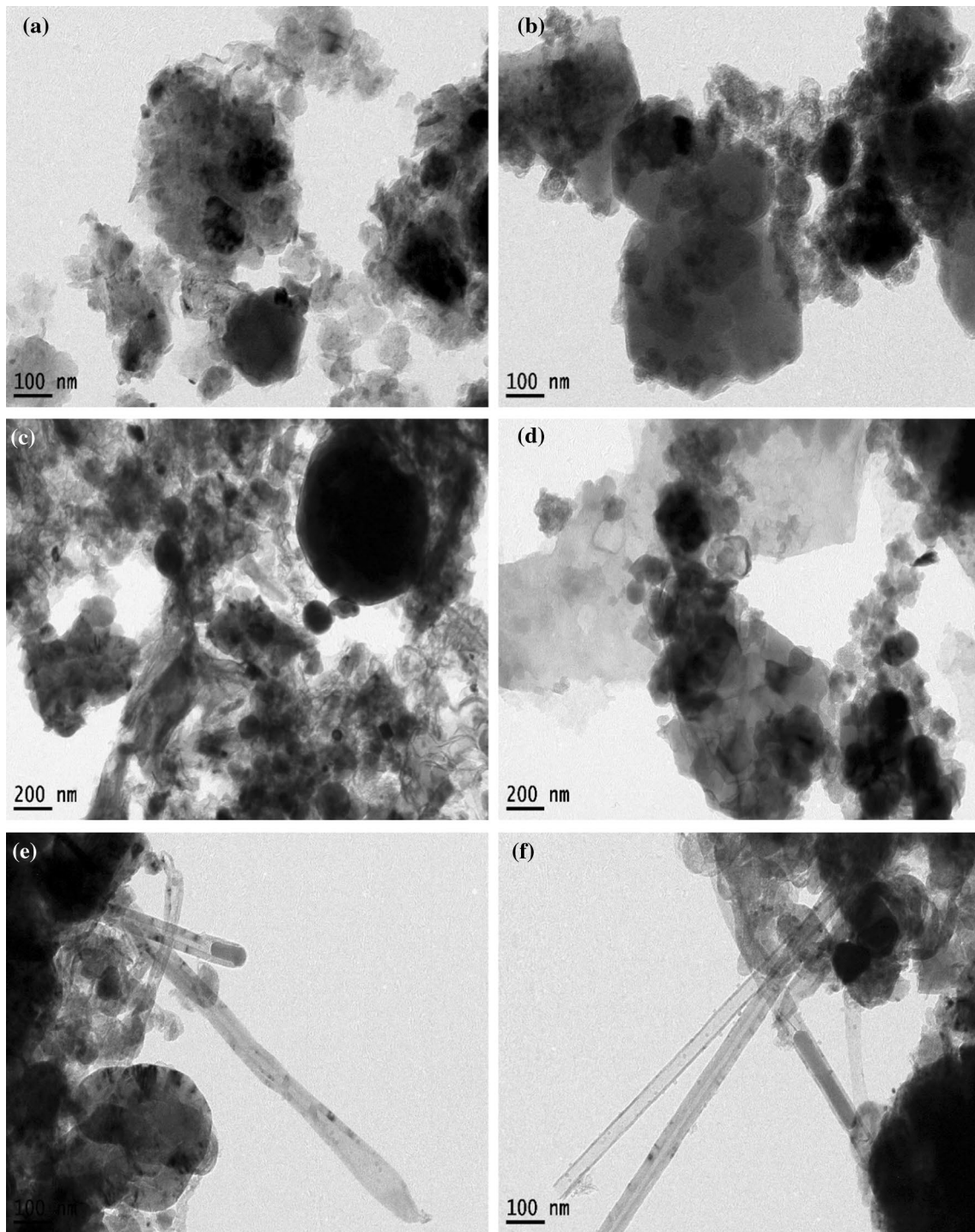
Fig. 1 TEM micrographs of CP. **a** 500, **b** 600, **c** 700, **d** 800, **e** 900, **f** 1000

CNT can be produced from HDPE pyrolysis depending on the reaction temperature. From TEM measurement, the CNT has a total diameter of about 70 nm and an internal diameter of 44 nm, while from SEM measurement, the largest CMS has a diameter of 14 μm. C–H–N–S elemental analysis of CP revealed the presence of high C% and the

Table 1 Textural properties of CP

| Sample	BET surface area $(m^2\,g^{-1})$	Total pore volume $(cm^3\,g^{-1})$	Mean pore diameter (nm)
CP-500	16.17	0.099	26.7
CP-600	14.07	0.095	26.9
CP-700	10.26	0.091	28.0
CP-800	9.65	0.084	30.9
CP-900	9.03	0.081	36.1
CP-1000	8.32	0.082	39.2

Fig. 2 SMZ adsorption efficiency of prepared adsorbents

reduction of H (w%) via removal of hydrogen during the scission of C–H with temperature (Table 1S). The EDX analysis was conducted to confirm the purity of CP. The pyrolysis of HDPE produces high-purity carbon materials; CP-500 to CP-1000 contains 95.9, 94.1, 93.49, 87.33, 84.01, 81.62 wt% of carbon, respectively, with a limited amount of oxygen (Fig. S3a-f). Traces of iron, chromium, and copper reported in the EDX spectra are possibly due to the thermal corrosion of the stainless-steel reactor or additive and impurities in the plastic. Such metals may act as catalysts to facilitate CNT synthesis at 900 and 1000 °C (Zhuo and Levendis 2014).

Figure S4 shows the XRD analysis of CP where the peaks at 2θ of 24°, 26°, 30°, 36°, 42.6°, 49°, 57°, and 63° are attributed to the diffraction planes of carbon, while the peaks at 2θ of 33° and 63° are possibly due to metals such as copper, chromium, and iron detected by EDX analysis (Kun et al. 2011; Wong et al. 2016). The peaks at 2θ of 24–26°, 42.6°, and 49° are standard intrinsic peaks corresponding to the (002), (100), and (101) diffraction planes of graphene (Mensah et al. 2021). The (101) diffraction plane depicts a stacking order of graphene sheets (Joseph Berkmans et al. 2014; Mensah et al. 2021). The flat peaks in CP-500 depict amorphous graphene and a lack of carbon growth. The formation of amorphous graphene as observed in the broad and flat peaks is due to the termination of sp2-hybridized bonds of carbon atoms or cross-linking of the hexagonal planar units by oxygen that was present during the carbonization, hence disrupting any order in the graphitic plane (Shen and Lua 2013; Mensah et al. 2021). Such graphite typically has diffuse sets of inter-layer distances that are averagely larger than those in crystalline graphite (Shen and Lua 2013). From CP-600 to CP-1000, the carbon XRD peaks intensified and became sharper, especially the peaks at 2θ of 24°, 26°, and 35°. This peak intensification indicates an improvement in both graphitization and carbon growth with temperature.
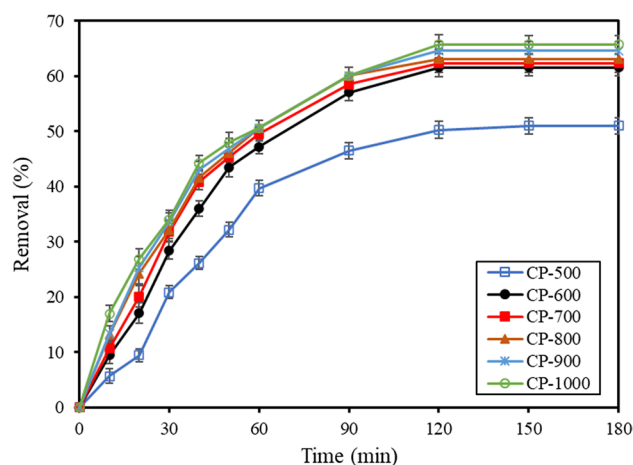
The N_2 adsorption–desorption isotherms and pore distribution are illustrated in Fig. S5, while the BET specific surface area, average pore diameter, and total pore volume of CP are summarized in Table 1. According to the IUPAC classification, the typical type-III isotherm was observed for N_2 adsorption–desorption isotherms (Fig. S5a), suggesting a mesoporous texture of all CP. The pore size distributions (Fig. S5b) revealed that the CP contained broadly distributed pores with sizes generally below 40 nm. CP's surface area and pore volume decreased with temperature (CP-500 > > CP-1000) due to agglomeration of graphene sheets and CMS formation with temperature. Moreover, the increasing temperature increased the pore diameters due to the dominant occurrence of the pore widening effect than
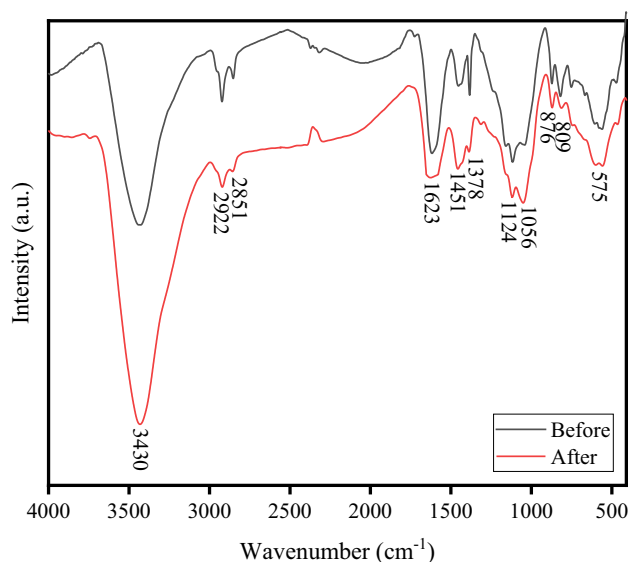
Fig. 3 FTIR spectra of CP-600 before and after adsorption

the pore opening effect, further resulting in a decrease of the specific surface area and pore volume (Shokry et al. 2019).

Adsorption efficiency of prepared carbon materials

The prepared carbon materials from the pyrolysis of HDPE waste at 500 to 1000 °C were tested for their adsorptive ability for SMZ in solution. From Fig. 2, the SMZ removal was enhanced with increasing pyrolysis temperature of the prepared adsorbents (CP-1000 > CP-900 > CP-800 > CP-700 > CP-600 > CP-500). This trend can be attributed to improved graphitization (high aromatic C=C bonds) with increasing pyrolysis temperatures. Since SMZ adsorption occurred via π–π electron interactions, graphitization of the adsorbents enhanced the interaction between the adsorbate and the adsorbents, improving the adsorption capacity. Moreover, impurity metals like iron in CP-800, CP-900, and CP-1000 can enhance SMZ adsorption via hydrogen bonding or complexation (Bai et al. 2021; Khenniche et al. 2021). However, no significant improvement in the adsorption capacity of the produced materials was observed at temperatures above 600 °C. Accordingly, CP-600 was selected as the best adsorbent for subsequent experiments. CP-600 achieved a removal efficiency of 62% in 180-min contact time. The SMZ adsorption was further confirmed by the presence of nitrogen (N) and sulfur (S) from SMZ ($C_{12}H_{14}N_4O_2S$) on CP-600 after adsorption (Fig. S6).

Role of functional groups in SMZ adsorption mechanism

The role of surface functional groups in an adsorption process can elucidate the adsorption mechanism (Mensah et al. 2022a). Thus, CP-600 was characterized by FTIR analysis before and after SMZ adsorption to identify fluctuations in its surface functional groups peaks that were possibly involved in the adsorption process (Fig. 3). The pristine CP-600 contained an FTIR peak at 1622 cm^{-1} due to the C=C stretching of benzene rings (El Essawy et al. 2017). This aromatic C=C structure is characteristic of graphitic carbon and suitable for hydrophobic interactions with pollutants in solution (El Essawy et al. 2017; Mensah et al. 2022a). The peak at 1387 cm^{-1} is attributed to the C–C skeletal vibration of the benzene ring (Yang et al. 2015). The O–H stretching vibration associated with the presence of molecular hydrogen bonds in polymeric compounds such as alcohols, carboxylic acids, and phenols, as well as lattice water, is assigned to the peak at 3430 cm^{-1} (Shokry et al. 2019; Mensah et al. 2022a). The peak at 2922 cm^{-1} is assigned to the C–H groups of uniform and ununiformed stretching vibrations of alkanes or alkyl groups (Ahmad et al. 2015; Shokry et al. 2019). This finding was confirmed by the depletion of hydrogen content with temperature during the HDPE

pyrolysis as seen in the elemental analysis. The broad peak at 1340–910 cm^{-1} is ascribed to the C–O stretching in ester, ether, or phenol groups, while that of 1451 cm^{-1} is due to the C=O stretching of lactones, ketones, or carboxylic anhydrides (Ahmad et al. 2015). The peaks at 876 and 817 cm^{-1} are attributed to the C–H derivatives in the aromatic rings, and the peak at 575 cm^{-1} is due to the out-of-plane angular deformation of aromatic rings of CP-600 (Shokry et al. 2019).

After SMZ adsorption, the intensity of the C=C peak of CP-600 was reduced due to the interaction and stretching vibrations of SMZ's pyrimidine and aromatic C=C bonds. The benzene ring C–C skeletal vibrations peak intensity was also reduced due to interactions with the aromatic group of SMZ (Yang et al. 2015). This change confirms that the hydrophobic benzene rings of CP-600 interacted with the pyrimidine and aromatic rings of SMZ via π–π electron coupling or π^{+}–π electron donor–acceptor interactions (Mensah et al. 2022a). The intensified peak at 1463 and 1056 cm^{-1} is due to the scissoring vibration of the N–H bonds of the aromatic amine (-NH$_2$) group and S=O bonds of the sulfonamide (–S(=O)$_2$–NH) group of the SMZ, respectively, indicating that SMZ was adsorbed onto the surface of CP-600 (Hu et al. 2022). The slight changes in the oxygen functional groups' peaks of CP-600 after SMZ adsorption suggest that oxygen functional groups did not play a major role in the SMZ uptake. The increased O–H peak intensity is contributed by lattice water taken up during the SMZ adsorption or vibrations of the N–H bonds of the –NH$_2$ and –S(=O)$_2$–NH groups of SMZ (Hu et al. 2022).

Operational conditions of SMZ adsorption

Data analysis of SMZ adsorption

The design of experiment (DOE) approach was used to investigate the effect of pH, adsorbent dose and SMZ concentration on SMZ removal by CP-600. Unlike the one-factor-at-a-time (OFAT) approach, DOE like RSM can show that interaction between the factors of a process, requires fewer experiments to optimize the operating parameters, allows for sequential experimentation, and can be used to troubleshoot a process (Wahid and Nadir 2013; Samy et al. 2020b). Table 2 provides the detailed conditions of 20 experiments with the expected and measured removal percentages of SMZ in 120-min adsorption. The polynomial model in Eq. 3 represents the relationship between surface response (SMZ removal %) and the three operational conditions.

$$\begin{aligned} \text{SMZ removal } (\%) = {} & 149.5 - 3.70X - 19.05Y + 74.3Z \\ & + 0.1164X^2 + 0.619Y^2 - 16.2Z^2 \quad (3) \\ & - 0.075XY - 2.25XZ + 1.56YZ \end{aligned}$$

Table 2 Detailed conditions of adsorption experiments, measured removal efficiency from the experiments, and predicted removal efficiency from the surface response model

Run	Coded values of parameters			Measured values of parameters			SMZ removal	
	SMZ concentration	pH	Adsorbent dose	SMZ concentration	pH	Adsorbent dose	Measured	Predicted
1	1	1	1	12.5	9	0.7	26	25.9015
2	1	−1	1	12.5	5	0.7	71	66.8195
3	1	1	−1	12.5	9	0.3	10	8.2955
4	1	−1	−1	12.5	5	0.3	55	51.7095
5	−1	1	1	7.5	9	0.7	44	44.0115
6	−1	−1	1	7.5	5	0.7	85	83.4295
7	−1	1	−1	7.5	9	0.3	21	21.9055
8	−1	−1	−1	7.5	5	0.3	67	63.8195
9	−2	0	0	5.0	7	0.5	61	61.201
10	2	0	0	15.0	7	0.5	28	30.981
11	0	0	2	10.0	7	0.9	58	59.197
12	0	0	−2	10.0	7	0.1	20	21.981
13	0	2	0	10.0	11	0.5	13	11.669
14	0	−2	0	10.0	3	0.5	90	94.501
15	0	0	0	10.0	7	0.5	42	43.181
16	0	0	0	10.0	7	0.5	42	43.181
17	0	0	0	10.0	7	0.5	44	43.181
18	0	0	0	10.0	7	0.5	42	43.181
19	0	0	0	10.0	7	0.5	43	43.181
20	0	0	0	10.0	7	0.5	43	43.181

where X = SMZ concentration (mg/L), Y = pH and Z = adsorbent dose (g/L).

The model's applicability is shown by the high R^2 value (99.09%) and adjusted R^2 value (98.27%). Additionally, the low p-values and high F-values (Table S2) prove the significance of the model. Furthermore, the predicted SMZ removal deviated slightly from the measured removal, showing this model's consistency and reliability (Table 1).

Effect of operational conditions on SMZ removal

The interactions between the three operational parameters (SMZ concentration, adsorbent dose, and pH) investigated by RSM are illustrated in Fig. 4. According to the RSM model, the SMZ removal efficiency was influenced by the operating parameters in the degree of pH > adsorbent dose > SMZ concentration (based on F-values in Table S2).

Sulfonamides like SMZ are mobile ionizable antibiotics, and their speciation can change with solution pH (Wegst-Uhrich et al. 2014). SMZ can be cationic (SMZ^+), anionic (SMZ^-), non-ionic (SMZ^0), or zwitterionic ($SMT^\pm$) depending on the solution pH (Liu et al. 2017; Ameen et al. 2020). SMZ has pKa values of 2.28 (pKa$_1$) and 7.42 (pKa$_2$), indicating that there can be zwitterionic species if pH is between 2.28 and 7.42, cationic species when pH is less than 2.28, and anionic species when pH is more than 7.42

(Kurwadkar et al. 2007). This amphoteric behavior of SMZ occurs through the ionization of aromatic amine (-NH$_2$) and sulfonamide (–S(=O)$_2$–NH) groups of SMZ by protonation and deprotonation reactions as shown in Fig. S7a-d (Wegst-Uhrich et al. 2014; Tzeng et al. 2016; Ameen et al. 2020). Increasing pH, therefore, drastically reduced SMZ adsorption on CP-600. At pH values beyond the pH$_{pzc}$ of CP-600 (7.1) and Pka$_2$ of SMZ, CP-600 becomes deprotonated with a net negative charge, and there are intense repulsive forces between –S(=O)$_2$–N$^-$ group of SMZ$^-$ and [CP-600]$^-$. The adsorption of SMZ was enhanced in low pH (pH < pH$_{pzc}$) conditions. Previous studies have shown that SMZ^0, SMT$^+$, and SMZ$^\pm$ may coexist in mildly acidic conditions (Wegst-Uhrich et al. 2014; Tzeng et al. 2016). Thus, the improved adsorption of SMZ at pH between 4 and 6 occurred via π-π electron interactions between C=C bonds of SMZ^0/SMT$^+$/SMZ$^\pm$ and CP-600, electrostatic interaction between –S(=O)$_2$–N$^-$ groups of SMZ$^\pm$ and [CP-600]$^+$, and hydrogen bonding between –NH$_2$ and –S(=O)$_2$–NH groups of SMZ and CP-600 (Fig. 5). Although in extremely low pH = 3 high repulsive forces are expected to occur between [CP-600]$^+$ and -NH^{3+} group of SMZ$^+$, the adsorption of SMZ was enhanced in all acidic conditions. This improvement can be associated with SMZ^0, SMT$^\pm$, and SMZ$^+$ being electrophilic species (Xie et al. 2014; Tzeng et al. 2016). SMT$^\pm$ and SMZ$^+$ have stronger electron-withdrawing abilities (more electrophilic) due to their cationic amino groups
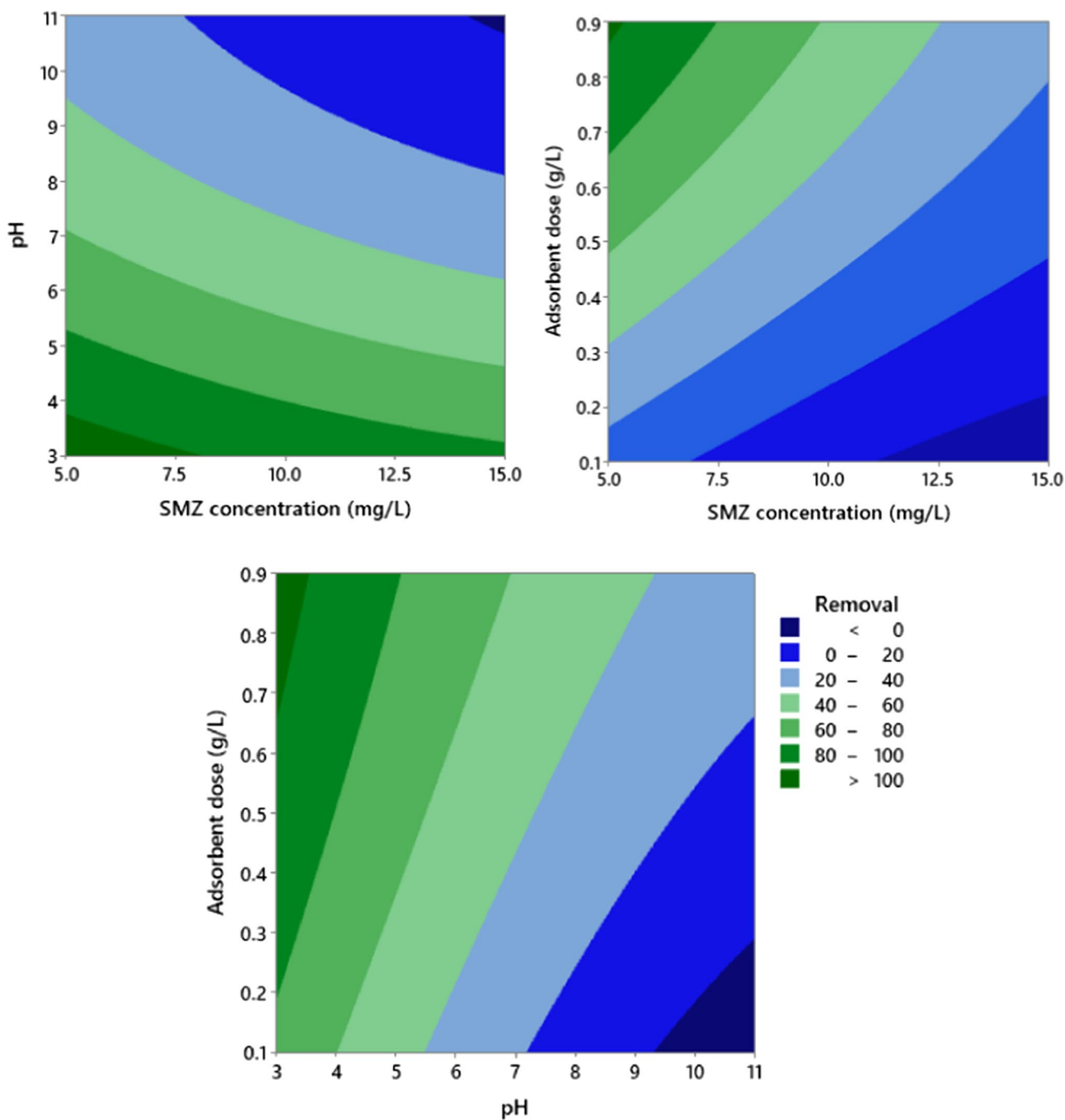
Fig. 4 Effect of operational conditions on SMZ removal efficiency

(-NH^{3+}) and thus are relatively effective π electron acceptors than SMZ$^-$ (Xie et al. 2014; Tzeng et al. 2016). Hence, the π electrons in the aromatic ring of SMT$^\pm$ and SMZ$^+$ would be polarized and the electron density would drop at low pH, leading to a simultaneous reduction in the electrostatic repulsion between the π electrons of SMZ's aromatic rings. Consequently, acidic conditions favored SMZ adsorption via π^+–π electron donor–acceptor interactions between

Fig. 5 SMZ adsorption mechanism on CP-600
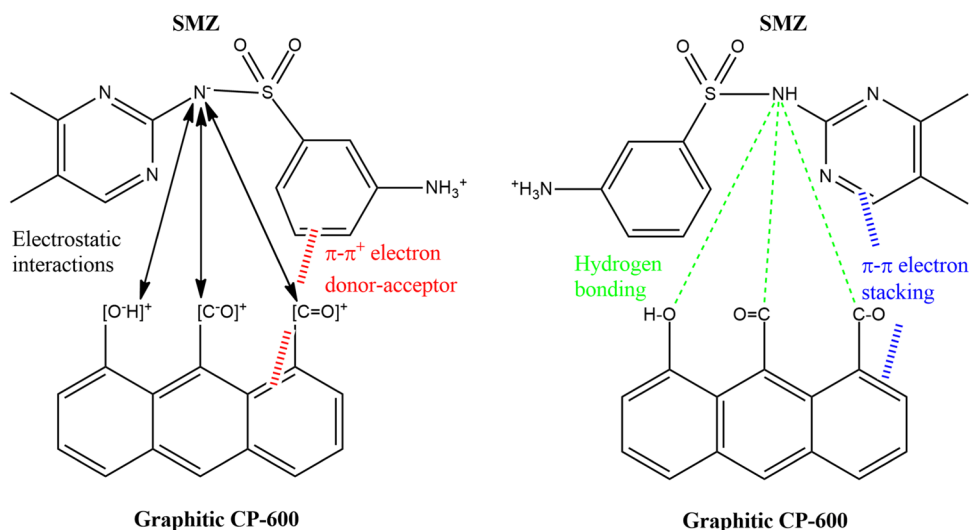
the polarized aromatic SMT$^\pm$ and SMZ$^+$ and the electron-rich aromatic rings of graphitic CP-600 as shown in Fig. 5. This conclusion is also established by the distinct changes in the FTIR peak of the C=C bonds of CP-600 after SMZ adsorption, as demonstrated in Fig. 3. As a result, electrostatic interactions and hydrogen bonding may not have been the main SMZ adsorption mechanism.

The adsorption efficiency of SMZ was enhanced with increasing CP-600 dose. Raising the CP-600 dose increases the interaction between the SMZ and the adsorbent by increasing the availability of active adsorption sites due to an increase in total surface area and the number of binding sites. Conversely, the equilibrium capacity toward SMZ (q_e) may decrease as the CP-600 dose increases. CP-600 particles may tend to aggregate much quicker as the adsorbent mass increases, and this can saturate adsorption sites, reduce adsorbents' total effective surface area, extend the diffusional path, and reduce the adsorption capacity.

Increasing SMZ concentration decreased the SMZ removal efficiency. Increasing SMZ concentration can increase the mass transfer driving force by increasing the number of collisions between SMZ molecules and the surface of the adsorbents. This phenomenon occurs during the early adsorption phase and can produce high adsorption capacities (Elkady et al. 2020). However, the ratio of available binding sites on CP-600 to the initial SMZ concentration diminished with increasing SMZ concentration and the adsorption sites became rapidly saturated, preventing further migration of the remaining SMZ toward the adsorbent's surface, and reducing the removal efficiency. Contrarily, the ratio of available binding sites to initial SMZ concentration is larger at lower SMZ concentrations, meaning that complete SMZ adsorption is more likely at the lower SMZ concentrations.

Table 3 Parameters and coefficients of the kinetic models for SMZ-sorption systems at temperature of 25 °C, pH of 3, and adsorbents dose of 0.9 g/100 mL

C_0 (mg/L)		15	30	60	120
q_e, exp		14.86	21.18	33.12	52.80
PFO	q_e, cal	20.08	26.51	46.95	40.19
	k_1	0.024	0.043	0.056	0.036
	R^2	0.949	0.948	0.933	0.930
	$\Delta q(\%)$	20.29	14.54	24.11	13.78
PSO	q_e, cal	18.04	24.66	36.97	57.32
	k_2	0.0016	0.0017	0.0016	0.0014
	R^2	0.990	0.993	0.996	0.998
	$\Delta q(\%)$	12.38	9.492	6.715	4.952
IPD	C	1.546	3.271	7.117	9.032
	K_{ipd}	1.14	1.61	2.41	3.58
	R^2	0.947	0.891	0.841	0.800
LFD	K_{lfd}	0.024	0.043	0.056	0.036
	R^2	0.949	0.948	0.933	0.930

The RSM optimization predicted optimal SMZ adsorption (99.99% removal) at an adsorbent dose = 0.9 g/L, SMZ concentration = 12.4 mg/L, and pH = 3 at 25 °C. These optimal conditions were validated by conducting a triplicate experiment under these conditions where an average SMZ removal of 98.85% was achieved.

SMZ adsorption behavior

SMZ adsorption kinetics and diffusion mechanism

The SMZ adsorption was rapid at the initial 60 min (Fig. S8). This fast reaction is due to the high porosity of the mesoporous graphitic CP-600 and the availability of active

sites. The porous nature of CP-600 promoted SMZ diffusion into the inner pores, where rapid adsorption took place. Moreover, graphene-based adsorbents react instantly with aromatic absorbate due to the π–π electron interactions (Mensah et al. 2022a). The adsorption of SMZ progressed steadily as active sites were occupied until 120 min when equilibrium was achieved and no substantial increase in the adsorption capacity was observed.

The values of the parameters of SMZ adsorption kinetics models are summarized in Table 3. The pseudo-second order (PSO) (Fig. S9a) fitted the SMZ adsorption on CP-600 with higher R^2 values ($R^2 = 0.990–0.998$) than pseudo-first order (PFO) (Fig. S9b) ($R^2 = 0.930–0.949$) and Elovich (ELV) model (Fig. S9c) ($R^2 = 0.971–0.913$). Additionally, the PSO calculated equilibrium adsorption capacities (qe, cal) were closer to the experimental adsorption capacities with lower $\Delta q(\%)$ error values than PFO. This PSO behavior suggests that the interactions between SMZ and functional groups on CP-600 surface controlled the adsorption capacity and the adsorption is centered on equilibrium adsorption, which is determined by the quantity of SMZ adsorbed onto CP-600's surface and the quantity of SMZ adsorbed at equilibrium (Ebelegi et al. 2020).

The intraparticle diffusion constant, k_{id}, improved with increasing the initial SMZ concentration due to rising interactions between the SMZ molecules and the CP-600 active sites (Table 3). Likewise, the thickness of the boundary layer increased due to the increasing SMZ concentration. The intraparticle diffusion model fitted fairly well with the SMZ adsorption (0.800–0.947), and the mechanism of SMZ diffusion is illustrated with the intraparticle diffusion model as depicted in Fig. S10a. The adsorption process had three phases. The first phase included the diffusion of SMZ molecules into the large mesopores, which happened at the adsorbent's outer surfaces (Mensah et al. 2022a). The second phase is diffusion from the surface to the internal sites. This stage is regulated by intraparticle diffusion and is the steady adsorption stage (Mensah et al. 2022a). The third and last phase is the equilibrium stage, which is the slowest step (Mensah et al. 2022a). However, since its linear plots did not have zero intercepts, it is possible that intraparticle diffusion may not be the only rate-controlling step (Ahmad et al. 2015; Khan et al. 2018). The liquid film diffusion model (Fig. S10b) fitted better on the adsorption kinetics (0.930–0.949) and was closer to the zero intercept. Hence, it is concluded that the liquid film diffusion controlled the early rapid adsorption stage, while the second stage was intraparticle diffusion (Ahmad et al. 2015).

Table 4 Adsorption isotherm parameters for SMZ-adsorbent systems at an adsorbent dosage of 1 g/100 mL, pH of 3, and temperature of 25 °C

Adsorption isotherm	Parameter	Value
Langmuir (linear)	q_m	60.55
	k_L	0.066
	R_L	0.132
	R^2	*0.923*
Langmuir (nonlinear)	R^2	*0.954*
Freundlich (linear)	k_F	11.50
	n_F	3.065
	R^2	*0.977*
Freundlich (nonlinear)	R^2	*0.963*
L-F	q_{mLF}	235.3
	k_{LF}	8.891
	n_{LF}	0.477
	R^2	*0.951*
Temkin	k_T	1.857
	B_T	9.347
	R^2	*0.835*
R-P	$A (10^6)$	1.924
	$B (10^5)$	2.212
	β	0.587
	R^2	*0.952*
Sips	$S (10^{-5})$	1.008
	$k_S (10^5)$	8.600
	β_S	0.413
	R^2	*0.955*
D–R	q_{DR}	47.12
	k_{DR}	1.570
	$\beta_{ad} \times 10^{-7}$	2.558
	E	1.398
	R^2	*0.591*
Toth	q_{mTH}	4.967
	k_{TH}	0.995
	n_{TH}	0.677
	R^2	*0.999*
Ra-P	q_{mP}	0.116
	$k_P (10^4)$	3.432
	m_P	0.587
	R^2	*0.960*

SMZ adsorption isotherm

The adsorption isotherms were fitted on the equilibrium plot as shown in Fig. S11, and the values of the isotherms' parameters are given in Table 4. The n_F value was greater than unity, while the R_L value was less than unity, indicating that the SMZ adsorption on CP-600 was favorable (Al-Ghouti and Da'ana 2020). CP-600 has a maximum Langmuir adsorption capacity (q_m) of 60.55 mg/g. The

SMZ adsorption followed the linear Freundlich isotherm model (Fig. S12a) with a higher coefficient of determination than the linear Langmuir model (Fig. S12b). However, the nonlinear Freundlich model ($R^2 = 0.963$) and Langmuir ($R^2 = 0.962$) were both better fit to the equilibrium plot than the L-F ($R^2 = 0.951$), Temkin ($R^2 = 0.835$), Redlich-Peterson ($R^2 = 0.952$), and Sips ($R^2 = 0.955$) models. The Dubinin-Radushkevich (D–R) isotherm model was also applied to describe the pore filling mechanism and physical or chemical nature of the adsorption process (Khan et al. 2018). The D–R constant (β_{ad}) and D–R apparent energy of adsorption (E) were estimated using Eqs. 4 and 5 (Khan et al. 2018):

$$E = \frac{1}{\sqrt{2\beta_{ad}}} \tag{4}$$

$$\beta_{ad} = \frac{k_{DR}}{R^2 T^2} \tag{5}$$

The D–R model had a weak correlation ($R^2 = 0.591$) with equilibrium SMZ adsorption on CP-600 and thus could not confirm any physisorption or pore filling. However, the heterogeneity of CP-600 surface energy was affirmed by the Toth parameter, $n_{TH} \neq 1$, and Radke-Prausnitz parameter, $m_P \neq 0$ (Ayawei et al. 2017; Al-Ghouti and Da'ana 2020).

SMZ adsorption thermodynamics

The thermodynamic fitting and parameters are presented in Fig. S13 and Table S3, respectively. Since the ΔH is positive, the adsorption reaction was endothermic. The negative ΔG values imply that adsorption reactions were spontaneous and viable. Furthermore, the ΔG values declined with increasing temperature, implying that the adsorption process was more spontaneous with temperature and chemisorption (Mensah et al. 2022a). Therefore, the Freundlich behavior of the adsorption isotherm may be more of surface heterogeneity than physical adsorption. The positive ΔS signifies that the adsorption process's randomness increased near the solid–liquid interface. A positive S value also alludes to a solvent-replacing mechanism in the absorption, in which SMZ molecules substitute water molecules on the surface of the adsorbents.

Reusability of CP-600

After SMZ adsorption, CP-600 was collected via filtration and centrifugation, and the adsorbed SMZ was desorbed by washing CP-600 in methanol and then distilled water (Hu et al. 2022). The eluted CP-600 was dried at 100 C for 3 h and reused. The reusability of CP-600 was conducted

Table 5 Comparison of recent SMZ adsorption studies

Adsorbent	q_m (mg/g)	Experimental conditions	Isotherm	Kinetics	Thermodynamics	Refs
Mesoporous graphitic carbon (CP-600)	60.55	t = 2 h; pH = 3; Ad = 0.9 g/L, C_o* = 120 mg/L	Langmuir and Freundlich	PSO, IPD and LFD	Endothermic, spontaneous	This work
Ferromagnetic activated carbon	28.73	t = 2 h, Ad = 0.5 g/L, C_0* = 50 mg/L	Freundlich	PSO, IPD and LFD	–	Khenniche et al. (2021)
nTiO$_2$/CNT	44.2	t = 24 h; pH = 5, C_o* = 50 mg/L	Langmuir and Freundlich	PSO, IPD and LFD	–	Xia et al. (2019)
Commercial activated carbon	3.0713	t = 24 h; Ad = 6 g/L, Co* = 100 mg/L	Langmuir and Temkin	PSO, IPD and membrane diffusion and internal diffusion	Exothermic, spontaneous	Liu et al. (2017)
FeCl$_3$-modified activated carbon	17.241	t = 24 h; Ad = 6 g/L, C_o* = 100 mg/L	Langmuir and Temkin	PSO, IPD and membrane diffusion and internal diffusion	Exothermic, spontaneous	Liu et al. (2017)
Multi-walled carbon nanotubes	38.13	t = 24 h; pH = 5; Ad = 0.32 g/L, C_o* = 100 mg/L	Langmuir	PSO, IPD	–	Yang et al. (2015)
Cow manure-based carbon	3.62	t = 12 h; pH = 3; Ad = 1 g/L, C_o* = 100 mg/L	Freundlich	PSO, IPD	–	Tzeng et al. (2016)
Highly porous carbon from α-cellulose	786.18	t = 24 h; pH = 6; Ad = 0.2 g/L, C_o* = 200 mg/L	Langmuir	PSO, IPD	Endothermic, spontaneous	Jinsong et al. (2016)

*where Ad = adsorbent dose

using the optimum conditions of 0.9 g/L adsorbent dose, 12.4 mg/L SMZ concentration and pH 3 at 25 °C. The trendline of Fig. S14 depicts a decline in the SMZ removal efficiency from the first (99%) to the fifth (71%) cycle. The multiple reuses of CP-600 can lead to a reduction in its activity as a result of lower active sites and specific surface area following regeneration; hence, the SMZ removal efficiency can drop (Hu et al. 2022). Moreover, the loss of CP-600 during collection via filtration and centrifugation can decrease SMZ removal efficiency (Mensah et al. 2022a). This problem with collection and adsorbent loss can be solved by magnetizing CP-600 (Mensah et al. 2022a).

Comparison with recent SMZ adsorbents

Table 5 compares this current work with literature under various SMZ adsorption experimental settings. CP-600 performed better with comparatively high SMZ adsorption capacity and fast kinetics (2-h adsorption equilibrium time) than other studies' adsorbents (Yang et al. 2015; Jinsong et al. 2016; Tzeng et al. 2016; Liu et al. 2017; Xia et al. 2019; Khenniche et al. 2021). Other adsorbents that appear to have a higher SMZ absorption capacity than CP-600 were chemically modified with reagents such as $FeCl_3$, which can add to the cost of SMZ adsorption and may be potentially noxious to the environment. Thus, this work's use of discarded plastics offers a unique, simple, ecological, and inexpensive approach to managing plastic waste while providing a facile one-pot solvent-free pyrolysis route of synthesizing carbon-rich materials for SMZ wastewater treatment.

Conclusion

The objectives of this work were achieved as follows:

1. This work proved the concept of plastic waste valorization into carbon-rich materials via a facile one-pot solvent-free pyrolysis route and successfully used the solid carbon product to remove SMZ from aqueous solution.
2. The carbon yield was enhanced with temperature, and the optimum yield was achieved at 600 °C.
3. The effect of temperature on the morphology, surface area, porosity, structure, and crystallinity of the produced chars was successfully investigated and discussed. Increasing temperature improved the CP's graphitization and the formation of CMS and CNT. The mean pore diameter of the CP increased slightly with temperature, while the opposite occurred with the total surface area and pore volume.
4. CP-600 showed good SMZ adsorption when all prepared adsorbents were tested for their adsorption capabilities toward SMZ.
5. An optimization study using RSM showed that the optimal operating conditions for achieving 99.99% removal were pH 3.0, a catalyst dose of 0.9 g/L, and an SMZ concentration of 12.4 mg/L.
6. SMZ adsorption was favorable in acidic conditions, and the mechanism occurred primarily through π–π electron stacking or π^+–π electron donor–acceptor interactions between C=C bonds in SMZ and that of the prepared graphitic adsorbent. Electrostatic interactions and hydrogen bonding were secondary adsorption mechanisms.
7. The SMZ adsorption followed the PSO better than PFO and ELV. Both Langmuir and Freundlich models were good fit for the SMZ adsorption isotherm. Mutually, LFD and IPD controlled the diffusion mechanism of the adsorption. The adsorption process was endothermic and spontaneous.
8. CP-600 was reusable in five cycles.
9. The prepared CP-600 in this work exhibited higher adsorption capacity and faster kinetics than most adsorbents used in SMZ adsorption, indicating the potential for large-scale application.

The use of plastic waste in this work can eliminate the cost of purchasing precursors like coal, thereby reducing cost. Moreover, the valorization in this work provides an excellent solution to managing the environmental pollution from waste plastics through simple, green, and profitable technology. It is recommended that further studies be conducted to:

- Assess the potential of upcycling other types of plastic into carbon-based adsorbents for SMZ removal.
- Test adsorptive ability of CP-600 to remove other antibiotics, micropollutants, heavy metals, and real wastewater.
- Magnetize CP-600 to enhance its recyclability.
- Perform detailed economic analysis to evaluate the profitability of the technology.

Declarations

Conflict interests The authors have no relevant financial or non-financial interests to disclose.

Ethics approval This article does not contain any studies with human participants or animals performed by any of the authors.

Consent to participate Not applicable.

Consent for publication All authors have checked the manuscript and have agreed to publish this work in the International Journal of Environmental Science and Technology (IJEST).

References

Adel A, Alalm MG, El-Etriby HK, Boffito DC (2020) Optimization and mechanism insights into the sulfamethazine degradation by bimetallic ZVI/Cu nanoparticles coupled with H2O2. J Environ Chem Eng. https://doi.org/10.1016/j.jece.2020.104341

Ahmad MA, Ahmad N, Bello OS (2015) Modified durian seed as adsorbent for the removal of methyl red dye from aqueous solutions. Appl Water Sci 5:407–423. https://doi.org/10.1007/s13201-014-0208-4

Al-Ghouti MA, Da'ana DA, (2020) Guidelines for the use and interpretation of adsorption isotherm models: A review. J Hazard Mater 393:122383. https://doi.org/10.1016/j.jhazmat.2020.122383

Ameen HM, Kunsági-Máté S, Noveczky P et al (2020) Adsorption of sulfamethazine drug onto the modified derivatives of carbon nanotubes at different pH. Molecules. https://doi.org/10.3390/molecules25112489

Asante BNP, Nimako KO, Mensah K, et al (2020) Calcination behaviour of nsuta pyrolusite ore in the presence and absence of end-of-life polystyrene. In: Proceedings of the 6th UMaT Bienn Int Min Miner Conf 281–288

Ayawei N, Ebelegi AN, Wankasi D (2017) Modelling and interpretation of adsorption isotherms. J Chem. https://doi.org/10.1155/2017/3039817

Bai S, Zhu S, Jin C et al (2021) Sorption mechanisms of antibiotic sulfamethazine (SMT) on magnetite-coated biochar: pH-dependence and redox transformation. Chemosphere 268:128805. https://doi.org/10.1016/j.chemosphere.2020.128805

Bolívar-Subirats G, Rivetti C, Cortina-Puig M et al (2021) Occurrence, toxicity and risk assessment of plastic additives in Besos river. Spain Chemosp 263:128022. https://doi.org/10.1016/j.chemosphere.2020.128022

Dankwah JR, Koshy P (2014) Effect of HDPE addition on the pre-reduction of Mn3O4 to MnO by metallurgical coke. High Temp Mater Process 33:345–353. https://doi.org/10.1515/htmp-2013-0069

Dutta S, Gupta B, Srivastava SK, Gupta AK (2021) Recent advances on the removal of dyes from wastewater using various adsorbents: a critical review. Mater Adv 2:4497–4531

Ebelegi AN, Ayawei N, Wankasi D (2020) Interpretation of adsorption thermodynamics and kinetics. Open J Phys Chem 10:166–182. https://doi.org/10.4236/ojpc.2020.103010

El Essawy NA, Ali SM, Farag HA et al (2017) Green synthesis of graphene from recycled PET bottle wastes for use in the adsorption of dyes in aqueous solution. Ecotoxicol Environ Saf 145:57–68. https://doi.org/10.1016/j.ecoenv.2017.07.014

Elkady M, Shokry H, Hamad H (2020) New activated carbon from mine coal for adsorption of dye in simulated water or multiple heavy metals in real wastewater. Materials (basel). https://doi.org/10.3390/ma13112498

Eriksen M, Lebreton LCM, Carson HS et al (2014) Plastic pollution in the world's oceans: more than 5 trillion plastic pieces weighing over 250,000 Tons Afloat at Sea. PLoS ONE. https://doi.org/10.1371/journal.pone.0111913

Plastic Europe (2018) Plastics – the facts. Plast – Facts 2018

Geyer R, Jambeck JR, Law KL (2017) Production, use, and fate of all plastics ever made - supplementary information. Sci Adv 3:19–24

Hahladakis JN, Velis CA, Weber R et al (2018) An overview of chemical additives present in plastics: Migration, release, fate and environmental impact during their use, disposal and recycling. J Hazard Mater 344:179–199. https://doi.org/10.1016/j.jhazmat.2017.10.014

Hu X, Huang Y, Pan Z et al (2022) Preparation of carbonyl, hydroxyl, and amino-functionalized microporous carbonaceous nanospheres from syrup-based waste to remove sulfamethazine. Environ Sci Pollut Res. https://doi.org/10.1007/s11356-021-18375-5

Inyang MI, Gao B, Yao Y et al (2016) A review of biochar as a low-cost adsorbent for aqueous heavy metal removal. Crit Rev Environ Sci Technol 46:406–433

Isobe A, Uchiyama-Matsumoto K, Uchida K, Tokai T (2017) Microplastics in the Southern Ocean. Mar Pollut Bull 114:623–626. https://doi.org/10.1016/j.marpolbul.2016.09.037

Jinsong H, Jiangdong D, Zhang T et al (2016) Preparation of highly porous carbon from sustainable a-cellulose for superior removal performance of tetracycline and sulfamethazine from water. RSC Adv 6:28023–28033. https://doi.org/10.1039/c6ra00277c

Joseph Berkmans A, Jagannatham M, Priyanka S, Haridoss P (2014) Synthesis of branched, nano channeled, ultrafine and nano carbon tubes from PET wastes using the arc discharge method. Waste

Manag 34:2139–2145. https://doi.org/10.1016/j.wasman.2014.07.004

Khan EA, Shahjahan KTA (2018) Adsorption of methyl red on activated carbon derived from custard apple (Annona squamosa) fruit shell: Equilibrium isotherm and kinetic studies. J Mol Liq 249:1195–1211. https://doi.org/10.1016/j.molliq.2017.11.125

Khenniche L, Chemache Z, Saidou-Souleymane M, Aissani-Benissad F (2021) Elimination of antibiotics by adsorption on ferromagnetic carbon from aqueous media: regeneration of the spent carbon. Int J Environ Sci Technol. https://doi.org/10.1007/s13762-021-03808-y

Kühn S, Bravo Rebolledo EL, Van Franeker JA (2015) Deleterious effects of litter on marine life. In: Marine anthropogenic litter. Springer International Publishing, pp 75–116

Kun P, Wéber F, Balázsi C (2011) Preparation and examination of multilayer graphene nanosheets by exfoliation of graphite in high efficient attritor mill. Cent Eur J Chem 9:47–51. https://doi.org/10.2478/s11532-010-0137-5

Kurwadkar ST, Adams CD, Meyer MT, Kolpin DW (2007) Effects of sorbate speciation on sorption of selected sulfonamides in three loamy soils. J Agric Food Chem 55:1370–1376. https://doi.org/10.1021/jf060612o

Lebreton L, Andrady A (2019) Future scenarios of global plastic waste generation and disposal. Palgrave Commun 5:1–11. https://doi.org/10.1057/s41599-018-0212-7

Liu Y, Liu X, Dong W et al (2017) Efficient adsorption of sulfamethazine onto modified activated carbon: a plausible adsorption mechanism. Sci Rep 7:1–12. https://doi.org/10.1038/s41598-017-12805-6

Mahanna H, Samy M (2020) Adsorption of reactive red 195 dye from industrial wastewater by dried soybean leaves modified with acetic acid. Desalin Water Treat 178:312–321. https://doi.org/10.5004/dwt.2020.24960

Martínez-Sánchez C, Robles I, Godínez LA (2022) Review of recent developments in electrochemical advanced oxidation processes: application to remove dyes, pharmaceuticals, and pesticides. Springer, Berlin

Mensah K, Mahmoud H, Fujii M, Shokry H (2021) Upcycling of polystyrene waste plastics to high value carbon by thermal decomposition. Key Eng Mater 897:103–108. https://doi.org/10.4028/www.scientific.net/KEM.897.103

Mensah K, Mahmoud H, Fujii M, Shokry H (2022a) Novel nano-ferromagnetic activated graphene adsorbent extracted from waste for dye decolorization. J Water Process Eng 45:102512–102523. https://doi.org/10.1016/j.jwpe.2021.102512

Mensah K, Samy M, Ezz H et al (2022b) Utilization of iron waste from steel industries in persulfate activation for effective degradation of dye solutions. J Environ Manage 314:115108. https://doi.org/10.1016/j.jenvman.2022.115108

Mulla SI, Bagewadi ZK, Faniband B et al (2021) Various strategies applied for the removal of emerging micropollutant sulfamethazine: a systematic review. Environ Sci Pollut Res. https://doi.org/10.1007/s11356-021-14259-w

Nimako KO, Dwumfour A, Mensah K et al (2020) Calcination behaviour of Nsuta rhodochrosite ore in the presence and absence of end-of-life high density polyethylene. Ghana Min J 20:22–35. https://doi.org/10.4314/gm.v20i2.4

Poirier LA, Doerge DR, Gaylor DW et al (1999) An FDA review of sulfamethazine toxicity. Regul Toxicol Pharmacol 30:217–222. https://doi.org/10.1006/rtph.1999.1348

Pol VG (2010) Upcycling: converting waste plastics into paramagnetic, conducting, solid, pure carbon microspheres. Environ Sci Technol 44:4753–4759. https://doi.org/10.1021/es100243u

Pol VG, Thiyagarajan P (2009) Measurement of autogenous pressure and dissociated species during the thermolysis of mesitylene for the synthesis of monodispersed, pure, paramagnetic carbon particles. Ind Eng Chem Res 48:1484–1489. https://doi.org/10.1021/ie8014928

Pol VG, Thiyagarajan P (2010) Remediating plastic waste into carbon nanotubes. J Environ Monit 12:455–459. https://doi.org/10.1039/b914648b

Pol SV, Pol VG, Sherman D, Gedanken A (2009a) A solvent free process for the generation of strong, conducting carbon spheres by the thermal degradation of waste polyethylene terephthalate. Green Chem 11:448–545. https://doi.org/10.1039/b819494g

Pol VG, Calderon-Moreno JM, Thiyagarajan P (2009b) Catalyst-free, one-step synthesis of olivary-shaped carbon from olive oil. Ind Eng Chem Res 48:5691–5695. https://doi.org/10.1021/ie900095v

Powell B, W, (2019) The effect of plastic pollution on marine life. Pegasus Found 1:43–45

Rashid R, Shafiq I, Akhter P et al (2021) A state-of-the-art review on wastewater treatment techniques: the effectiveness of adsorption method. Environ Sci Pollut Res 28:9050–9066. https://doi.org/10.1007/s11356-021-12395-x

Rhodes CJ (2018) Plastic pollution and potential solutions. Sci Prog 101:207–260. https://doi.org/10.3184/003685018X15294876706211

Rochman CM, Browne MA, Underwood AJ et al (2016) The ecological impacts of marine debris: unraveling the demonstrated evidence from what is perceived. Ecology 97:302–312. https://doi.org/10.1890/14-2070.1

Samy M, Alalm MG, Mossad M (2020a) Utilization of iron sludge resulted from electro-coagulation in heterogeneous photo-fenton process. Water Pract Technol 15:1228–1237. https://doi.org/10.2166/wpt.2020.093

Samy M, Ibrahim MG, Alalm MG, Fujii M (2020) Modeling and optimization of photocatalytic degradation of methylene blue using lanthanum vanadate. Mater Sci Forum. https://doi.org/10.4028/www.scientific.net/MSF.1008.97

Samy M, Ibrahim MG, Gar Alalm M, Fujii M (2020c) Effective photocatalytic degradation of sulfamethazine by CNTs/LaVO4 in suspension and dip coating modes. Sep Purif Technol. https://doi.org/10.1016/j.seppur.2019.116138

Samy M, Gar Alalm M, Fujii M, Ibrahim MG (2021) Doping of Ni in MIL-125(Ti) for enhanced photocatalytic degradation of carbofuran: Reusability of coated plates and effect of different water matrices. J Water Process Eng 44:102449. https://doi.org/10.1016/j.jwpe.2021.102449

Shen Y, Lua AC (2013) A facile method for the large-scale continuous synthesis of graphene sheets using a novel catalyst. Sci Rep 3:1–6. https://doi.org/10.1038/srep03037

Shindhal T, Rakholiya P, Varjani S et al (2021) A critical review on advances in the practices and perspectives for the treatment of dye industry wastewater. Bioengineered 12:70–87

Shokry H, Elkady M, Hamad H (2019) Nano activated carbon from industrial mine coal as adsorbents for removal of dye from simulated textile wastewater: Operational parameters and mechanism study. J Mater Res Technol 8:4477–4488. https://doi.org/10.1016/j.jmrt.2019.07.061

Thushari GGN, Senevirathna JDM (2020) Plastic pollution in the marine environment. Heliyon 6:e04709. https://doi.org/10.1016/j.heliyon.2020.e04709

Tournier V, Topham CM, Gilles A et al (2020) An engineered PET depolymerase to break down and recycle plastic bottles. Nature 580:216–219. https://doi.org/10.1038/s41586-020-2149-4

Tzeng TW, Liu YT, Deng Y et al (2016) Removal of sulfamethazine antibiotics using cow manure-based carbon adsorbents. Int J Environ Sci Technol 13:973–984. https://doi.org/10.1007/s13762-015-0929-4

Van Franeker JA, Law KL (2015) Seabirds, gyres and global trends in plastic pollution. Environ Pollut 203:89–96. https://doi.org/10.1016/j.envpol.2015.02.034

Wahid Z, Nadir N (2013) Improvement of one factor at a time through design of experiments. World Appl Sci J 21:56–61. https://doi.org/10.5829/idosi.wasj.2013.21.mae.99919

Wegst-Uhrich SR, Navarro DAG, Zimmerman L, Aga DS (2014) Assessing antibiotic sorption in soil: A literature review and new case studies on sulfonamides and macrolides. Chem Cent J 8:1–12. https://doi.org/10.1186/1752-153X-8-5

Wong KT, Eu NC, Ibrahim S et al (2016) Recyclable magnetite-loaded palm shell-waste based activated carbon for the effective removal of methylene blue from aqueous solution. J Clean Prod 115:337–342. https://doi.org/10.1016/j.jclepro.2015.12.063

Xia T, Yan N, Li S et al (2019) Adsorption of tylosin and sulfamethazine by carbon nanotubes and titanium dioxide nanoparticles: pH-dependent mechanisms. Colloids Surfaces A Physicochem Eng Asp 581:123851. https://doi.org/10.1016/j.colsurfa.2019.123851

Xie M, Chen W, Xu Z et al (2014) Adsorption of sulfonamides to demineralized pine wood biochars prepared under different thermochemical conditions. Environ Pollut 186:187–194. https://doi.org/10.1016/j.envpol.2013.11.022

Yang Q, Chen G, Zhang J, Li H (2015) Adsorption of sulfamethazine by multi-walled carbon nanotubes: Effects of aqueous solution chemistry. RSC Adv 5:25541–25549. https://doi.org/10.1039/c4ra15056b

Zhang H, Pap S, Taggart MA et al (2018) A review of the potential utilisation of plastic waste as adsorbent for removal of hazardous priority contaminants from aqueous environments. Environ Pollut 258:1–12. https://doi.org/10.1016/j.envpol.2019.113698

Zhuang S, Zhu X, Wang J (2020) Adsorptive removal of plasticizer (dimethyl phthalate) and antibiotic (sulfamethazine) from municipal wastewater by magnetic carbon nanotubes. J Mol Liq 319:114267. https://doi.org/10.1016/j.molliq.2020.114267

Zhuo C, Levendis YA (2014) Upcycling waste plastics into carbon nanomaterials: A review. J Appl Polym Sci 131:1–14. https://doi.org/10.1002/app.39931